Nano Research

Open Access

Research Article

Magnetic-assisted self-powered vehicle motion sensor based on triboelectric nanogenerator for real-time monitoring of vehicle motion states

Xiaohui Lu[1,§], Chunyang Wang[1,2,§], Hancheng Li[1,§], Hengyu Li[2], Wei Lv[3], Shitong Yang[1], Shaosong Li[1], Jianming Wen[4] ✉, Bangcheng Zhang[5] ✉, and Tinghai Cheng[1,2] ✉

[1] *School of Mechatronic Engineering, Changchun University of Technology, Changchun 130012, China*
[2] *Beijing Institute of Nanoenergy and Nanosystems, Chinese Academy of Sciences, Beijing 101400, China*
[3] *Key Laboratory of Advanced Structural Materials, Ministry of Education and Advanced Institute of Materials Science, Changchun University of Technology, Changchun 130012, China*
[4] *College of Engineering, Zhejiang Normal University, Jinhua 321004, China*
[5] *School of Mechanical and Electrical Engineering, Changchun Institute of Technology, Changchun 130103, China*
[§] *Xiaohui Lu, Chunyang Wang, and Hancheng Li contributed equally to this work.*

Cite this article: *Nano Research*, **2025**, *18*, 94907015. https://doi.org/10.26599/NR.2025.94907015

ABSTRACT: The monitoring of vehicle motion states is a key factor to ensure smooth, safe, and efficient management of traffic in intelligent transportation systems. However, employing multiple sensors for vehicle motion states monitoring not only increases system costs but also complicates the wiring. Here, we propose an integrated magnetic-assisted self-powered vehicle motion sensor (MSVMS) based on a triboelectric nanogenerator for real-time monitoring of vehicle motion states, including acceleration, angular speed, and inclination angle. By introducing a magnetic repulsion adjustment system, the sensor can achieve automatic resetting and effectively monitor the vehicle's motion state during normal driving. Experimental results indicate that the electromagnetic generator (EMG) unit can achieve a maximum peak power of 4.5 mW at an optimal load resistance of 1 kΩ. Meanwhile, the triboelectric nanogenerator (TENG) unit demonstrated good sensing performance for acceleration, angular speed, and inclination angle, with fitting coefficients of 0.99, 0.979, and 0.978, respectively. Finally, the feasibility of the MSVMS in monitoring acceleration magnitude and direction is verified in a vehicle motion sensing system and actual vehicle test scenarios. This work further validates the potential application prospects of MSVMS in intelligent transportation systems.

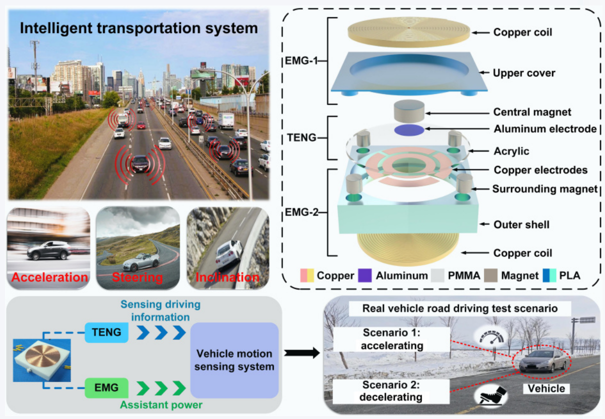

KEYWORDS: triboelectric nanogenerator, self-powered sensing, magnetic repulsion adjustment system, vehicle motion sensing system, real-time monitoring

1 Introduction

With the rapid development of urban traffic and the increasing number of vehicles, the importance of real-time monitoring of vehicle motion states has become increasingly prominent [1–4]. By monitoring the real-time state parameters of vehicles, the intelligent transportation system can accurately grasp the road conditions and vehicle movement, enabling information interaction between vehicles and providing crucial road condition information for drivers and intelligent driving systems. This plays an important role in alleviating traffic congestion, improving vehicle safety, and optimizing traffic efficiency [5–8]. At present, for the monitoring of vehicle motion states, the vehicle is usually equipped with speed sensor [9], acceleration sensor [10, 11], steering angle sensor [12, 13], tilt angle sensor [14], and other monitoring means to ensure

Received: July 17, 2024; **Revised:** August 20, 2024
Accepted: August 29, 2024

✉Address correspondence to Jianming Wen, wjming@zjnu.cn; Bangcheng Zhang, zhangbangcheng@ccut.edu.cn; Tinghai Cheng, chengtinghai@binn.cas.cn

that the driver can fully grasp the operation states of the vehicle. While these sensors have superior performance, employing multiple sensors with diverse functions for monitoring vehicle motion states can escalate system costs and necessitate intricate wiring [15]. In addition, these sensors require an external power supply, and the demand for additional power inevitably increases the vehicle's power consumption and environmental pollution [16]. Therefore, it is of great significance to develop a multi-functional, integrated, and self-powered vehicle motion sensor.

In 2012, Wang's research group proposed triboelectric nanogenerator (TENG) based on the coupling principle of contact electrification and electrostatic induction [17, 18]. The TENG not only effectively converts mechanical energy into electrical energy [19–22], but also shows potential application potential in the field of self-powered sensing [23–26]. Based on TENG, researchers have designed a series of self-powered sensors for vehicle state monitoring [27–29]. For example, Liu et al. developed a self-powered acceleration sensor with grating structure for monitoring vehicle motion [30], and Pang et al. proposed a self-powered three-dimensional (3D) acceleration sensor for monitoring vehicle collision acceleration [31]. Although the reported acceleration sensors have excellent acceleration sensing performance in one-dimensional and 3D space, they only have a single function (limited to acceleration sensing). In addition, Le et al. proposed a water-based TENG, which can realize two functions: wheel speed and road slope monitoring, showing wider application potential [32]. However, solid–liquid contact is sensitive to environmental conditions, which presents certain limitations. In the actual driving process, the vehicle usually exhibits a variety of motion states, and a single-function sensor can no longer meet the needs of vehicle state monitoring. Therefore, designing a self-powered vehicle motion sensor with multifunctional capabilities (such as acceleration, inclination angle, and angular speed sensing) is significant for monitoring vehicle motion states.

Herein, we present a magnetic-assisted self-powered vehicle motion sensor (MSVMS) based on a TENG for real-time monitoring of vehicle motion states, including acceleration, angular speed, and inclination angle. The electromagnetic generator (EMG) unit and TENG unit were integrated into a device through a magnetic repulsion adjustment system, thereby realizing energy harvesting and self-powered sensing of the MSVMS. Firstly, the output performance of the EMG and TENG units was tested, verifying the energy harvesting and self-powered sensing capabilities of the MSVMS. Experimental results show that the MSVMS can achieve a peak power of 4.5 mW and can monitor the magnitude and direction of acceleration, angular speed, and inclination angle in real-time. Finally, by constructing a vehicle motion sensing system and verifying it in the actual vehicle test scenario, the feasibility of MSVMS in monitoring acceleration in the actual vehicle operating environment is proved. This work further promotes the application of triboelectric sensors in vehicles.

2 Results and discussion

2.1 Structure design and working principle of MSVMS

The MSVMS is primarily used in the intelligent transportation system (Fig. 1(a)) to monitor the real-time driving attitude information of vehicles. This includes acceleration, angular speed, and inclination angle. The overall schematic diagram and detailed internal distribution of the MSVMS are shown in Fig. 1(b). The MSVMS is composed of two main parts: the EMG power generation unit (EMG unit) and TENG sensing unit (TENG unit).

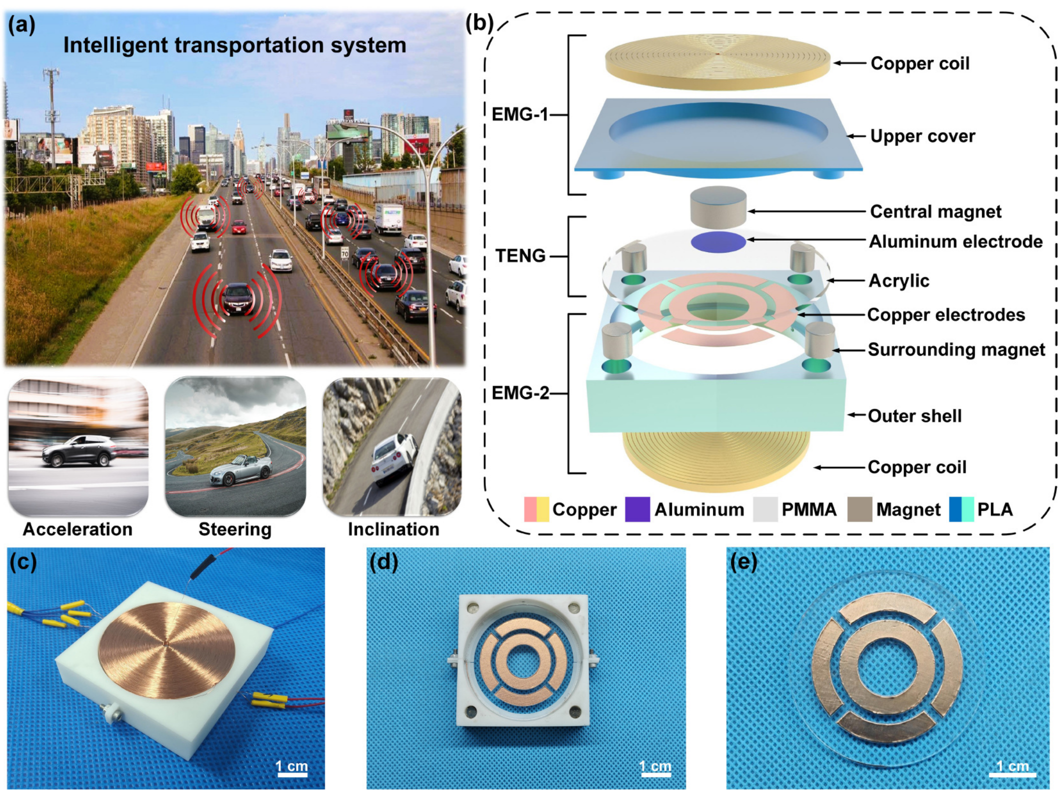

Figure 1 Design and application of the MSVMS. (a) Applications of the MSVMS in vehicles. (b) Internal detail diagram of the MSVMS. (c) Photograph of the designed MSVMS. (d) Photograph of the component structure. (e) Photograph of the electrode details.

The entire shell is made of 3D-printed polylactic acid (PLA) and features four equal-sized cylindrical hollow spaces near the four corners to hold surrounding magnets. The interior of the whole structure is a cylindrical space, in which the freely sliding central magnet and the copper coils, arranged in series at the top and bottom, a magnetic repulsion adjustment established with the central magnet and surrounding magnets, ensuring the central magnet remains in the initial central position without external excitation. The TENG unit comprises a central magnet and four surrounding magnets. The underside of the central magnet is covered with an aluminum film, serving as the positive triboelectric material, while the negative triboelectric layer is made of acrylic (polymethyl methacrylate (PMMA)). The acrylic plate is equipped with five copper electrodes, including a ring electrode and four arc electrodes (Back-E, Left-E, Forward-E, and Right-E). When the external excitation acts on the MSVMS, the central magnet moves in the cavity and contacts with the friction material on the acrylic plate to generate an electrical signal. The MSVMS prototype is shown in Fig. 1(c). Additionally, Figs. 1(d) and 1(e) illustrate the arrangement and details of the copper electrodes. The specific size parameters are shown in Fig. S1 in the Electronic Supplementary Material (ESM). Due to the external motion excitation, the detailed theoretical analysis of the various motion states of the central magnet is shown in Fig. S2 and Note S1 in the ESM.

The working principle of the MSVMS can be explained by the movement in the horizontal direction (Fig. 2(a)). In the absence of external excitation, the central magnet remains centered on the acrylic plate to maintain equilibrium. However, if the excitation occurs from any direction other than vertical, a horizontal force will break the equilibrium, forcing the central magnet to slide on the acrylic plate. In these processes, the open-circuit voltage can be detected on the copper electrode according to the triboelectric effect. When the central magnet slides on the acrylic plate, due to the different friction polarities of aluminum and acrylic around the magnet, electrons will be transferred from aluminum to the acrylic plate, resulting in positive and negative charges on their surfaces, respectively. When the central magnet is kept in its initial position (Fig. 2(a)(i)), there is no charge transfer between the copper electrode and the earth due to electrostatic balance. Once the Al electrode on the central magnet approaches the copper electrode (Fig. 2(a)(ii)), the positive friction charge will drive electrons from the ground to the copper electrode until the Al electrode is aligned with the copper electrode to achieve a new electrostatic balance (Fig. 2(a)(iii)). When the central magnet continues to slide forward to break the balance (Fig. 2(a)(iv)), the electrons in the copper electrode will flow back to the ground, and finally the central magnet returns to its initial position due to the magnetic repulsion. The copper electrode's open-circuit voltage will change with the movement of the central magnet during the whole movement.

To further explain the voltage generation principle of the EMG unit, the finite element electromagnetic simulation was carried out (Figs. 2(b)(i)–2(b)(iii)). By moving the central magnet to different positions, the magnetic flux density distribution in the vertical direction of the central magnet is obtained, which can observe the influence of the central magnet on other magnets around and the change of magnetic flux density. Simultaneously, to verify the electrical characteristics of the MSVMS, the electrostatic simulation of the sensor triboelectric module was carried out. The simulation results are schematically illustrated in Figs. 2(c)(i)–2(c)(iv). COMSOL simulates the electrostatic voltage distribution when the central magnet moves to different positions. This simulation confirms the mode of electrostatic potential distribution when the moving central magnet is regarded as an equipotential body. Therefore, by analyzing the copper electrode's open-circuit voltage, the motion parameters and modes of the central magnet can be detected.

2.2 Output performance of the EMG unit

To investigate the electrical output of the EMG unit at various vibration frequencies, the LinMot linear motor was employed as the

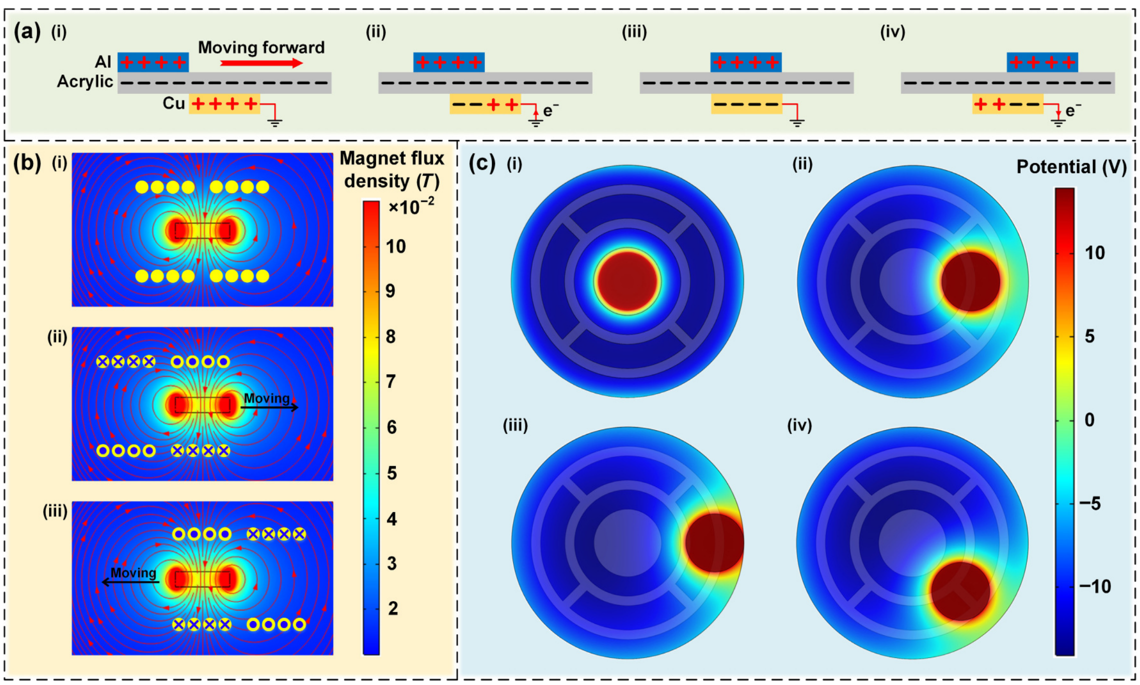

Figure 2 Working principle and simulation results of the MSVMS. (a) Schematic diagram of working principle of TENG sensing unit. (b) Finite element method magnetic simulation results of the EMG unit. (c) Electrostatic potential distributions of the central magnet at different positions.

external vibration excitation source, and different vibration frequencies are obtained by adjusting the parameters of the linear motor. Figure 3 shows the electrical characterization of the EMG unit in the MSVMS. The layered schematic structure of the internal components of the sensor is schematically illustrated in Fig. 3(a). A central magnet that slides freely within a cylindrical space, together with copper coils connected in series at the top and bottom, constitutes an EMG unit. Figure 3(b) illustrates the arrangement of the energy capture device (EMG power generation unit) and the sensing device (TENG sensing unit) within the sensor. The variation in magnetic flux density at the center of the EMG coil with the displacement of the central magnet is presented in Fig. 3(c). Furthermore, Figs. 3(d) and 3(e) present the schematic illustrations of the open-circuit voltage and short-circuit current waveforms of the EMG unit under 5 Hz linear motion excitation. The relationship between the open-circuit voltage and the input acceleration and input frequency is shown in Fig. 3(f). In this experimental test, the MSVMS is excited along the linear horizontal direction with different frequencies and accelerations. When the peak acceleration is 2*g* and the excitation frequency is 10 Hz, the maximum open-circuit voltage measured by the EMG unit is 7.61 V. By observing the relationship between the open-circuit voltage of the EMG unit with different input accelerations and input frequencies, an approximate linear increment between the measured open-circuit voltage and the input acceleration and frequency can be obtained. The collected energy is used to charge a capacitor of 100–820 μF (Fig. 3(g)), which further illustrates the energy collection capability and applicability of the EMG unit. The performance of the EMG unit was assessed in an actual working environment, and its voltage and current were measured under different load resistances (Fig. 3(h)). With an increasing load resistance, the voltage rises while the current decreases. Figure 3(i) schematically exemplifies the dependence of the peak output power of the EMG unit on different load conditions. At the optimal load resistance of 1 kΩ, the EMG unit achieves a maximum peak power capture of 4.5 mW.

2.3 Acceleration sensing performance of the TENG unit

The vehicle motion sensor can provide more accurate and comprehensive motion perception for the vehicle, help the vehicle to monitor and adapt to various driving conditions and dynamic changes in real-time, and improve the safety and comfort of driving. By monitoring the acceleration of the vehicle, dangerous driving behaviors such as sudden parking, quick start, and sudden braking can be detected in time. Therefore, as a vehicle motion sensor, it is necessary to explore the relationship between its electrical output and acceleration value.

To match the change of vehicle acceleration in daily driving, LinMot linear motor was used to adjust different acceleration values to verify the monitoring ability of MSVMS for acceleration (Fig. 4).

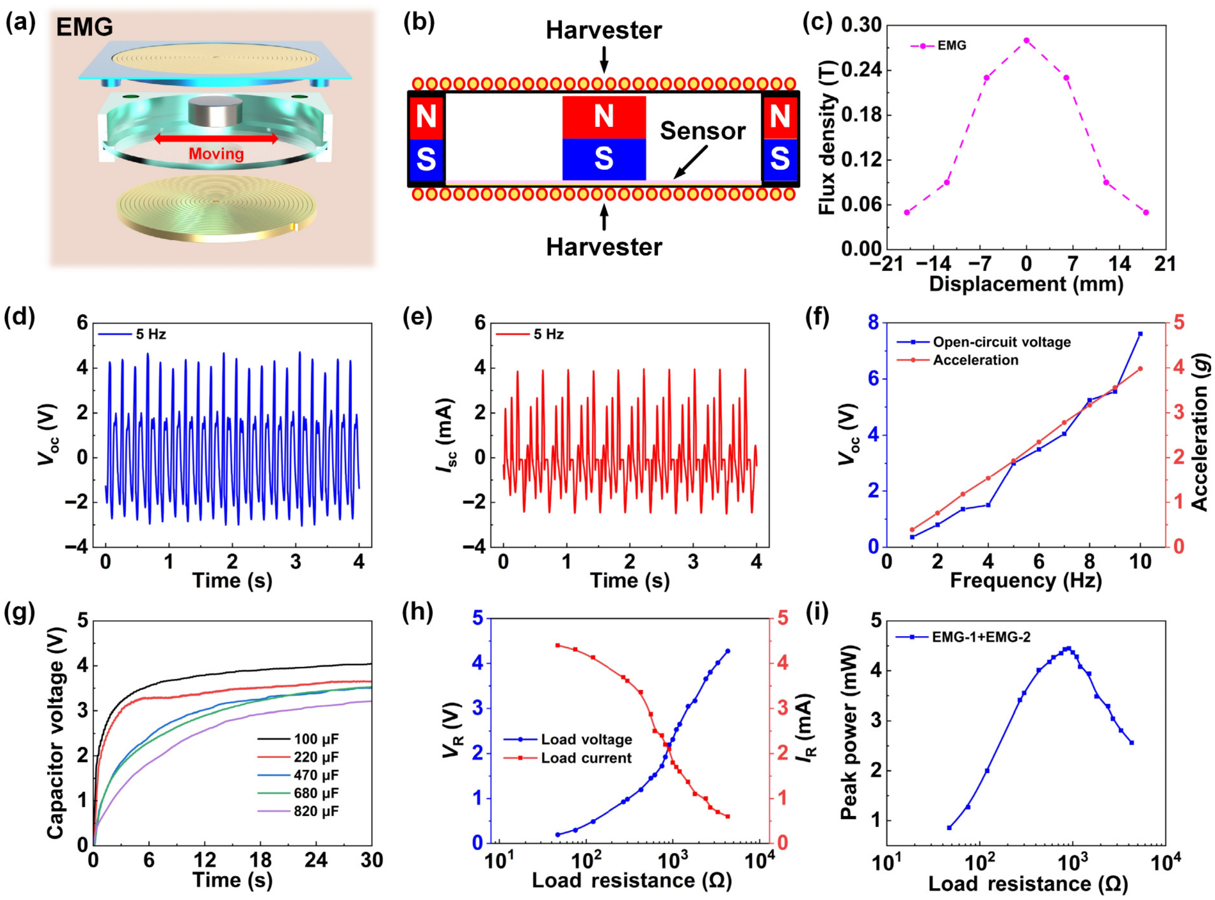

Figure 3 Electrical characterization of EMG unit. (a) Layered schematic diagram of the internal structure of EMG unit. (b) Detailed layout of sensing and energy harvesting in EMG unit. (c) Flux density diagram at the center of EMG coil at different positions of the magnet. (d) and (e) The output waveforms of open-circuit voltage and short-circuit current of EMG unit under 5 Hz linear motion excitation. (f) Dependence of open-circuit voltage of EMG on input acceleration and frequency. (g) The charging voltage curve of EMG charging different capacitors with time. (h) Voltage and current curves under different resistance loads. (i) Peak output power curves of EMG1 and EMG2 under different resistance loads.

清华大学出版社 Tsinghua University Press | SciOpen

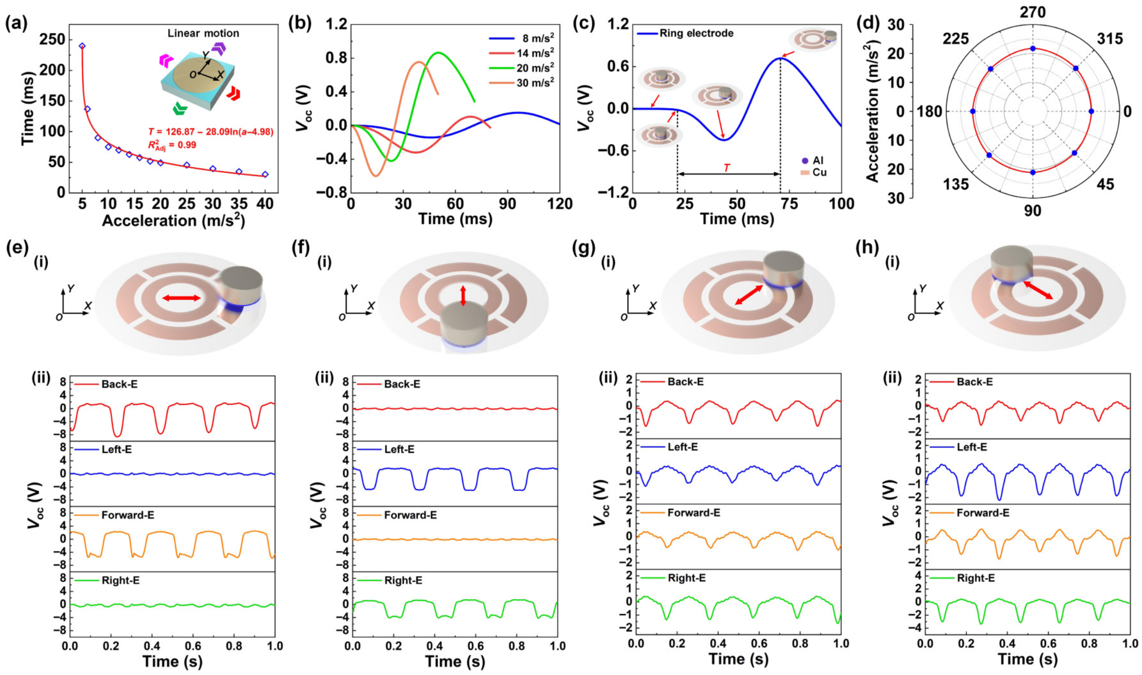

Figure 4 The working principle of the MSVMS linear acceleration measurement. (a) The relationship between acceleration and response time. (b) The open-circuit voltage curve of the sensor under variable acceleration. (c) The open-circuit voltage curve generated by the ring electrode under the acceleration of 1.8*g*. (d) Detected acceleration with the sensor moving in different directions with a fixed acceleration of 20 m/s². (e)–(h) Direction diagrams of eight linear motions and voltage waveforms of four arc electrodes.

When central magnet is stationary in the center position without being excited, the open-circuit voltage of ring electrode and arc electrode is 0. The open-circuit voltage of the ring electrode will first reach the valley value when the central magnet moves linearly in any direction and passes through ring electrode. When the central magnet moves away from the ring electrode towards the arc electrode, the ring electrode's open-circuit voltage will significantly increase, reaching a peak value. According to the time from the static open-circuit voltage value to the peak open-circuit voltage value, the time parameter T related to the acceleration can be determined as the response time. When the acceleration increases from 0 to 40 m/s², the signal response time of the ring electrode decays exponentially, and the relationship between the acceleration value a and the response time T is obtained (Fig. 4(a)). The open-circuit voltage of the MSVMS under 8, 14, 20, and 30 m/s² variable acceleration is shown in Fig. 4(b). Taking the open-circuit voltage curve generated by the ring electrode when collecting 1.8*g* acceleration as an example, the relationship between the characteristics of the voltage waveform and the motion position is shown in Fig. 4(c). The response time is the time of the open circuit voltage of the ring electrode from 0 to the trough of the curve and then to the peak. The response time of the ring electrode under different accelerations and the average response time of four consecutive repeated tests are shown in Fig. S3 in the ESM. Repeated experiments for four times show that the sensor has good repeatability. When the sensor moves forward and back along the X-axis, left and right along the Y-axis, and along the ± 45° direction with a fixed acceleration, the corresponding acceleration can be detected by the ring electrode in the TENG unit (Fig. 4(d)), indicating that the sensor has all-round monitoring ability in the horizontal direction.

The detection of the horizontal acceleration also includes the detection of the direction. Under the external linear excitation provided by the LinMot linear motor, the sensor performs linear motion accordingly. As shown in Figs. 4(e)–4(h), the tests of forward and back motion along the X-axis, left and right motion along the Y-axis, and ± 45° motion are carried out, and the open-circuit voltage curves of the arc electrodes in four directions are obtained. The experimental results show that when the central magnet moves forward and back along the X-axis (Fig. 4(e)), the central magnet first moves to the Back-E. Because of the influence of the magnetic repulsion, it will move back and forward along the X-axis, so the open-circuit voltage of the Back-E and the Forward-E will peak in turn. In contrast, the open-circuit voltage values of the Left-E and the Right-E are relatively small and remain unchanged. Therefore, the arc electrode with the voltage peak appearing first is the direction of motion of the central magnet. The situation of moving left and right along the Y-axis is similar (Fig. 4(f)). When the central magnet contacts Left-E and Right-E, the two arc electrodes of Left-E and Right-E appear voltage peaks successively. When the central magnet moves along the center line between two adjacent arc electrodes, such as linear motion along the 45° direction (Fig. 4(g)), the central magnet contacts both the Back-E and the Left-E, so the Back-E and the Left-E have the same electrostatic potential, and the Forward-E and the Right-E also produce the same electrostatic potential after a certain time interval. The results of linear motion in the 45° direction on the other side are similar (Fig. 4(h)). Through this electrode arrangement, the MSVMS can easily detect the direction of eight linear motions.

2.4 Angular speed and inclination angle sensing performance of the TENG unit

The monitoring of vehicle angular speed and inclination angle is an important means to ensure the safety and performance of the vehicle. It can help the vehicle system better adapt to different road conditions and driving modes, and improve the safety and comfort of driving. Due to the structural characteristics and electrode arrangement of the MSVMS, the sensor can also monitor the angular speed and inclination angle. When the MSVMS is placed in the rotation center, the central magnet inside it will always remain at the center of the circle. When the MSVMS is placed eccentrically, the central magnet will stay outside the center under the action of centrifugal force and magnetic repulsion. In practical applications, in addition to horizontal placement, the MSVMS can also realize angular speed monitoring by introducing the influence of gravity. By placing the MSVMS eccentrically on the rotating motor, the ability of the sensor to monitor the angular speed is analyzed. As shown in Fig. 5(a), when the central magnet rotates clockwise on the acrylic plate, Back-E, Left-E, Forward-E, and Right-E achieve their maximum output performance in turn. In the process of the central magnet's 90° rotation, only the Back-E produces high output, while all other arc electrodes produce low output voltage. Since the position of each arc electrode is separated equally by 90°, the output voltages of the Back-E, Left-E, Forward-E, and Right-E of the arc electrode in the MSVMS can be correlated by the corresponding rotation angles of 90°, 180°, 270°, and 360°, respectively. Therefore, the two continuous signal peaks indicate that the central magnet rotates by 90° and is denoted as $\Delta\theta$. The time difference between the two continuous signal peaks is denoted as Δt, and the ratio of $\Delta\theta$ to Δt is the value of angular speed. When the central magnet rotates counterclockwise on the acrylic plate, the frequency value (Fig. S4(h) in the ESM) was obtained by the fast Fourier transform (FFT) of the output waveform under different speeds. Figure 5(c) illustrates the linear relationship between frequency and angular speed, further proving the feasibility of the sensor for monitoring angular speed information. The experimental data for residual angular speed are shown in Figs. S4(a)–S4(g) in the ESM.

Then, the monitoring ability of the MSVMS for the value and direction of the inclination angle was explored. Most of the motion control programs in the vehicle are based on the *X*-axis and *Y*-axis for inclination angle monitoring. Therefore, a rotating motor test platform is established to make the MSVMS rotate along these two axes. First, rotating along the inclination axis (*Y*-axis) (Fig. 5(d)(i)), the Left-E and Right-E of the arc electrode produce high output voltages successively, and Back-E and Forward-E produce low output voltages (Fig. 5(d)(ii)). Then, rotating along the pitch axis (*X*-axis) (Fig. 5(e)(i)), the Back-E and Forward-E of the arc electrode produce high output voltages successively, and the output voltages of Left-E and Right-E of the arc electrode are lower (Fig. 5(e)(ii)). Therefore, the inclination direction is judged by the high output voltage peak of the four arc electrodes. Meanwhile, the open-circuit voltage values at different inclination angles were tested. The output voltage curves of different inclination angles are shown in Fig. 5(f). The inclination angle has a linear relationship with its output voltage (Fig. 5(g)). The linear fitting coefficient is 0.978, and the sensitivity of the inclination angle monitoring is 0.158 V/deg.

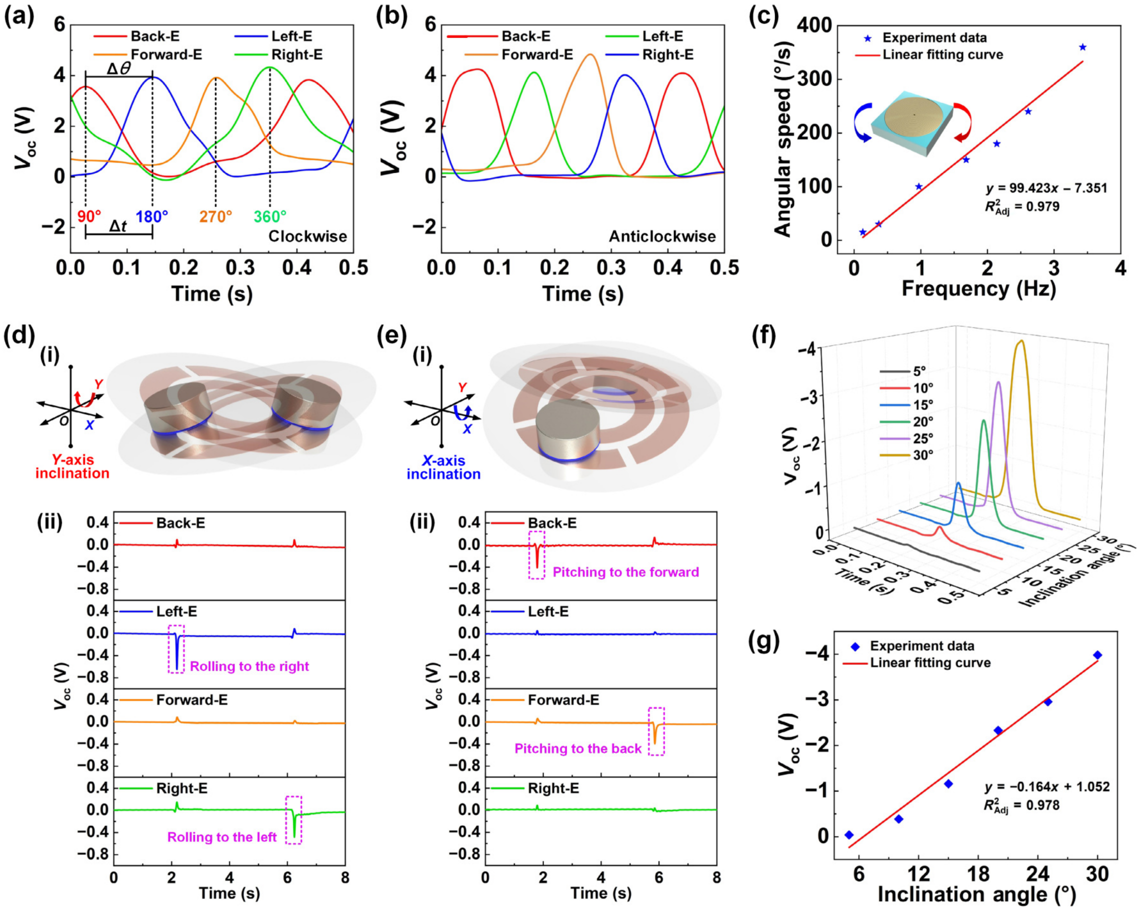

Figure 5 Working principle of the MSVMS angular speed and inclination angle measurement. (a) and (b) MSVMS open-circuit voltage waveforms of the four arc electrodes under clockwise and counterclockwise rotation motion excitation. (c) Relationship between angular speed and frequency. (d) MSVMS inclination along the *Y*-axis and voltage waveforms of four arc electrodes. (e) MSVMS inclination along the *X*-axis and voltage waveforms of four arc electrodes. (f) Open-circuit voltage of the MSVMS under different inclination angles. (g) Relationship between inclination angle and open-circuit voltage of the MSVMS.

2.5 Demonstration of MSVMS

To verify the feasibility of MSVMS in the field of vehicle sensing, a vehicle motion sensing system and a real vehicle test scene (Fig. 6(a)) are built. Considering the safety of the angular speed and inclination angle test scene, the real vehicle test scene only includes two scenes for monitoring acceleration. One is the acceleration monitoring when the vehicle steps on the accelerator, and the other is the deceleration monitoring when the vehicle steps on the brake. Through these two scenarios, the feasibility of the MSVMS for monitoring the magnitude and direction of acceleration in the real vehicle operating environment is verified.

The circuit design of the back-end integrated vehicle motion sensing system of the MSVMS is shown in Fig. 6(b). The EMG unit in the MSVMS is divided into two EMG units located above and below the sensor, named EMG1 and EMG2, respectively. EMG1 and EMG2 are stored in a 0.2 F capacitor C1 through rectification to provide direct current (DC) power for Arduino UNO-2. The TENG sensing unit in the MSVMS is divided into a ring electrode and four arc electrodes, which are named TENG1–TENG5. The TENG1 to TENG5 are rectified in parallel and connected to the A0–A4 serial port of Arduino UNO-1, and the filter capacitor CF is 0.1 μF, and then the stable voltage signal is given. A0 is connected to TENG1, which is the ring electrode and is responsible for processing the acceleration value information. A1–A4 is connected to TENG2-5, which is responsible for processing the acceleration direction information. The corresponding programming of the serial port can realize the function of signal processing. Finally, the complete acceleration information is displayed on the organic light-emitting diode (OLED) screen, and the signal processing and terminal display of the MSVMS by Arduino are verified as shown in Video S1 in the ESM. The back-end of the integrated vehicle motion sensing system is composed of the MSVMS main body, two Arduino UNO development boards as microcontrol unit (MCU), an energy storage capacitor, and an OLED screen as a terminal

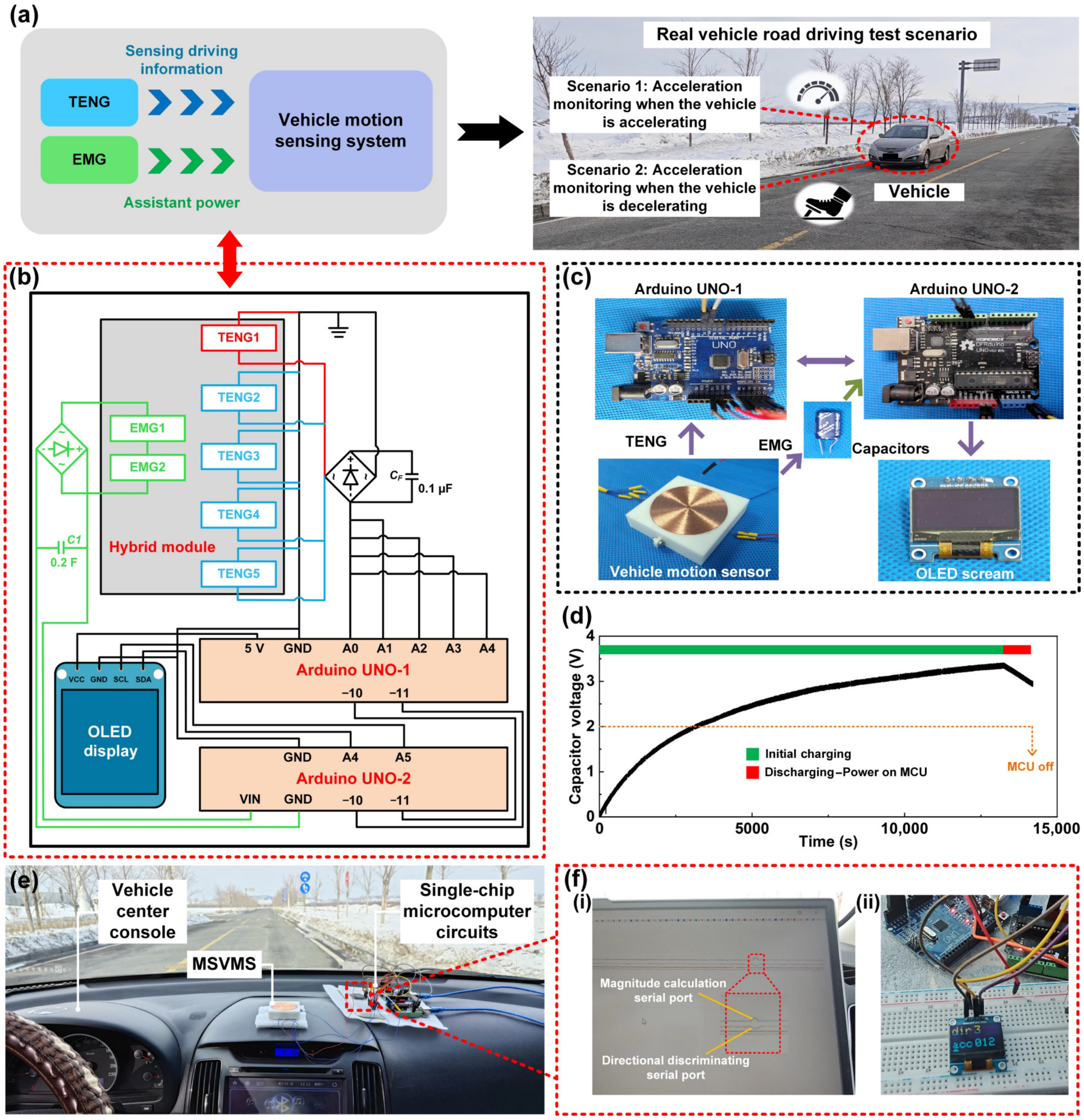

Figure 6 Application of the MSVMS in vehicles. (a) Working principle diagram and real vehicle test scene of integrated vehicle motion sensing system. (b) Circuit design diagram of the MSVMS back-end integrated vehicle motion sensing system. (c) Back-end circuit physical image of single chip microcomputer. (d) Capacitor charging and discharging voltage curve. (e) Real vehicle test scene for real-time monitoring of vehicle acceleration. (f) Vehicle real-time acceleration monitoring curve and results.

display (Fig. 6(c)). The upper computer is composed of a universal serial bus (USB) to transistor-transistor logic (TTL) serial port as an interface converter and a laptop that displays the received sensing signals. Figure 6(d) shows the discharge voltage curve of MSVMS charging 0.2 F capacitor at 3 Hz and operating MCU through the energy stored in the capacitor. The verification of the auxiliary power supply capability of the EMG unit in the MSVMS is shown in Video S2 in the ESM, which can successfully light 120 LED lights and power the temperature and humidity sensor. Next, a real vehicle acceleration test scenario (Fig. 6(e)) is built. The monitoring curves and results of vehicle acceleration and deceleration in the test link are shown in Fig. 6(f)(i), and the OLED screen (Fig. 6(f)(ii)) shows the acceleration magnitude and direction information measured in a demonstration experiment (the acceleration size is 12 m/s^2, and the direction is 3 (Forward-E)). The specific acceleration monitoring process is reflected in Video S3 in the ESM. The real vehicle test results show that integrated vehicle motion sensing system can monitor the acceleration transformation in real-time.

Finally, to highlight the feasibility of the application of the MSVMS in the actual vehicle environment, the durability experiment of the sensor and the performance experiment of the sensor under different humidity were carried out (Fig. S5 in the ESM). The results show that the open-circuit voltage amplitude of the ring electrode decays to the initial 84.3% (Fig. S5(a) in the ESM) after continuous operation for 6 h and continuous operation for 64,800 times. After continuous operation of the arc electrode for 6 h and continuous operation of 64,800 times, the open-circuit voltage amplitude is attenuated to the initial 90.3% (Fig. S5(b) in the ESM). Although the voltage amplitudes of the two electrodes have decreased, the decrease in voltage amplitude will not affect the system's extraction and analysis of the signal frequency, as both signal analyses are based on the frequency of the frictional electrical signal and the presence or absence of the signal. Next, the performance tests of the two electrodes under different relative humidity environments (Fig. S5(c) in the ESM) were carried out. The results show that the open-circuit voltages of the two electrodes continue to decrease with the increase of relative humidity, because the frequency of the triboelectric signal is used for signal analysis at the forward-end, the transformation of the voltage amplitude does not affect the extraction and analysis of the signal frequency. The humidity and durability tests show that MSVMS has broad application prospects in the field of vehicle motion monitoring.

3 Conclusions

In summary, a MSVMS based on triboelectric nanogenerators was proposed for real-time monitoring of vehicle motion states. Firstly, the power generation performance of the MSVMS was verified by experiments. Under the optimal load resistance of 1 kΩ, MSVMS can capture the peak power of 4.5 mW, which provides a potential solution to meet the power demand of real-time display of acceleration information. Subsequently, the sensing performance of MSVMS was tested. The experimental results show that MSVMS can effectively monitor the acceleration, angular speed, and tilt angle, and the fitting coefficients are 0.99, 0.979, and 0.978, respectively. In addition, in the constructed vehicle motion sensing system and the actual vehicle test scenario, the real-time monitoring ability of the system to the acceleration change during the actual operation of the vehicle is verified. Finally, the durability test of the sensor was carried out. After 6 h of continuous operation, the open-circuit voltage amplitude of the ring electrode of MSVMS attenuated to 84.3% of the initial value, but the frequency remained unchanged. This work not only demonstrates a self-powered vehicle motion sensor but also expands the commercialization and application of TENGs in the vehicle field.

4 Experimental section

4.1 Fabrication of MSVMS

The MSVMS had dimensions of 52 mm (length) × 52 mm (width) × 12.5 mm (height). The outer shell was made by 3D printing technology, and the 3D printing material was PLA. The four corners of the enclosure had four equal-sized cylindrical spaces for placing magnets (5 mm in diameter). The magnet material was rubidium ferroboron, the grade was N52. Two cylindrical spaces were arranged on the upper and lower sides of the shell to place the coil (44.5 mm in diameter), and the wire diameter of the coil was 0.1 mm. The thickness of the aluminum electrode on the central magnet (10 mm in diameter) was 80 μm, and the negative triboelectric layer (50 mm in diameter) was made by acrylic cutting technology. In addition, the thickness of the five copper electrodes on the acrylic was 80 μm, and the specific size was shown in Fig. S1 in the ESM.

4.2 Measurement of MSVMS

The performance test of MSVMS was driven by a linear motor (LinMot HF01 23) and a rotating motor (Mitsubishi Group, HG KR43J). The output signal of MSVMS was measured by data acquisition card (NI, USB 6356) and recorded by LabVIEW software. Finally, the Arduino UNO development board was used to read the sensor information and display it on the OLED screen.

Electronic Supplementary Material: Supplementary material (additional figures, notes and videos, the theoretical analysis of MSVMS) is available in the online version of this article at https://doi.org/10.26599/NR.2025.94907015.

Data availability

All data needed to support the conclusions in the paper are presented in the manuscript and the Electronic Supplementary Material. Additional data related to this paper may be requested from the corresponding author upon request.

Acknowledgements

This work was supported by the Beijing Natural Science Foundation (No. L244004), Beijing Natural Science Foundation (No. 3244038), and the Postdoctoral Fellowship Program (Grade B) of China Postdoctoral Science Foundation (No. GZB20230731)

Declaration of competing interest

All the contributing authors report no conflicts of interest in this work.

Author contribution statement

X. H. L.: Investigation, writing-original draft, and validation. C. Y. W.: Conceptualization, investigation, and writing – original draft. H. C. L.: Investigation, validation, and editing. H. Y. L.: Validation.

W. L.: Investigation. S. T. Y.: Investigation. S. S. L.: Validation. J. M. W.: Resources, writing – review & editing, and supervision. B. C. Z.: Conceptualization, resources, writing – review & editing, and supervision. T. H. C.: Conceptualization, resources, writing – review & editing, and supervision.

Use of AI statement

None.

References

[1] Singh, K. B.; Arat, M. A.; Taheri, S. Literature review and fundamental approaches for vehicle and tire state estimation. *Vehicle Syst. Dyn.* **2019**, *57*, 1643–1665.

[2] Jiang, F. H.; Dong, M. Y.; Fan, Y. Z.; Wang, Q. C. Research on motor speed control method based on the prevention of vehicle rollover. *Energies* **2022**, *15*, 3609.

[3] Du, Z. J.; Deng, M.; Lyu, N.; Wang, Y. G. A review of road safety evaluation methods based on driving behavior. *J. Traffic Transp. Eng. (Eng. Ed.)* **2023**, *10*, 743–761.

[4] Rodrigo Marco, V.; Kalkkuhl, J.; Raisch, J.; Scholte, W. J.; Nijmeijer, H.; Seel, T. Multi-modal sensor fusion for highly accurate vehicle motion state estimation. *Control Eng. Pract.* **2020**, *100*, 104409.

[5] Zhao, W.; Yin, J. T.; Wang, X. H.; Hu, J.; Qi, B. Z.; Runge, T. Real-time vehicle motion detection and motion altering for connected vehicle: Algorithm design and practical applications. *Sensors* **2019**, *19*, 4108.

[6] Guerrero-Ibáñez, J.; Zeadally, S.; Contreras-Castillo, J. Sensor technologies for intelligent transportation systems. *Sensors* **2018**, *18*, 1212.

[7] Zhang, R.; Zhang, Z. C.; Guan, Z. W.; Li, Y. F.; Li, Z. X. Autonomous lane changing control for intelligent vehicles. *Cluster Comput.* **2019**, *22*, 8657–8667.

[8] Pang, Y. F.; Zhu, X. Y.; Lee, C.; Liu, S. N. Triboelectric nanogenerator as next-generation self-powered sensor for cooperative vehicle-infrastructure system. *Nano Energy* **2022**, *97*, 107219.

[9] Corbrion, C.; Ditchi, T.; Holé, S.; Carreel, E.; Lewiner, J. A broad beam Doppler speed sensor for automotive applications. *Sens. Rev.* **2001**, *21*, 28–32.

[10] Jin, L.; Ma, S. Y.; Deng, W. L.; Yan, C.; Yang, T.; Chu, X.; Tian, G.; Xiong, D.; Lu, J.; Yang, W. Q. Polarization-free high-crystallization β-PVDF piezoelectric nanogenerator toward self-powered 3D acceleration sensor. *Nano Energy* **2018**, *50*, 632–638.

[11] Ramakrishnan, J.; Gaurav, P. T. R.; Chandar, N. S.; Sudharsan, N. M. Structural design, analysis and DOE of MEMS-based capacitive accelerometer for automotive airbag application. *Microsyst. Technol.* **2021**, *27*, 763–777.

[12] Woo, S. T.; Park, Y. B.; Lee, J. H.; Han, C. S.; Na, S.; Kim, J. Y. Angle sensor module for vehicle steering device based on multi-track impulse ring. *Sensors* **2019**, *19*, 526.

[13] Gao, J. C.; Petovello, M.; Cannon, M. E. Integration of steering angle sensor with global positioning system and micro-electro-mechanical systems inertial measurement unit for vehicular positioning. *J. Intell. Transp. Syst.* **2008**, *12*, 159–167.

[14] Benz, D.; Botzelmann, T.; Kück, H.; Warkentin, D. On low cost inclination sensors made from selectively metallized polymer. *Sens. Actuators A: Phys.* **2005**, *123–124*, 18–22.

[15] Leen, G.; Heffernan, D. Expanding automotive electronic systems. *Computer* **2002**, *35*, 88–93.

[16] Zhao, C.; Wang, Z. Y.; Wang, Y. W.; Qian, Z. A.; Tan, Z.; Chen, Q. Y.; Pan, X. X.; Xu, M. Y.; Lai, Y. C. MXene-composite-enabled ultra-long-distance detection and highly sensitive self-powered noncontact triboelectric sensors and their applications in intelligent vehicle perception. *Adv. Funct. Mater.* **2023**, *33*, 2306381.

[17] Fan, F. R.; Tian, Z. Q.; Wang, Z. L. Flexible triboelectric generator. *Nano Energy* **2012**, *1*, 328–334.

[18] Wang, Z. L.; Wang, A. C. On the origin of contact-electrification. *Mater. Today* **2019**, *30*, 34–51.

[19] Zhang, C.; Tang, W.; Han, C. B.; Fan, F. R.; Wang, Z. L. Theoretical comparison, equivalent transformation, and conjunction operations of electromagnetic induction generator and triboelectric nanogenerator for harvesting mechanical energy. *Adv. Mater.* **2014**, *26*, 3580–3591.

[20] Yang, W. Q.; Chen, J.; Jing, Q. S.; Yang, J.; Wen, X. N.; Su, Y. J.; Zhu, G.; Bai, P.; Wang, Z. L. 3D stack integrated triboelectric nanogenerator for harvesting vibration energy. *Adv. Funct. Mater.* **2014**, *24*, 4090–4096.

[21] Zhang, L.; Jin, L.; Zhang, B. B.; Deng, W. L.; Pan, H.; Tang, J. F.; Zhu, M. H.; Yang, W. Q. Multifunctional triboelectric nanogenerator based on porous micro-nickel foam to harvest mechanical energy. *Nano Energy* **2015**, *16*, 516–523.

[22] Ding, M. R.; Wang, J. L.; Zhao, D.; Li, H. Y.; Cheng, X. J.; Wen, J. M.; Wang, Z. L.; Cheng, T. H. Magnetic-field-assisted triboelectric nanogenerator for harvesting multi-directional wave energy. *Nano Res.* **2024**, *17*, 7144–7152.

[23] Wang, Z. L. Triboelectric nanogenerators as new energy technology and self-powered sensors-principles, problems and perspectives. *Faraday Discuss.* **2014**, *176*, 447–458.

[24] Askari, H.; Hashemi, E.; Khajepour, A.; Khamesee, M. B.; Wang, Z. L. Towards self-powered sensing using nanogenerators for automotive systems. *Nano Energy* **2018**, *53*, 1003–1019.

[25] Wang, B. C.; Zhai, X. Y.; Wei, X. L.; Shi, Y. P.; Huo, X. Q.; Li, R. N.; Wu, Z. Y.; Wang, Z. L. A self-powered and concealed sensor based on triboelectric nanogenerators for cultural-relic anti-theft systems. *Nano Res.* **2022**, *15*, 8435–8441.

[26] Pang, Y. F.; Zhu, X. Y.; Yu, Y.; Liu, S. N.; Chen, Y.; Feng, Y. Waterbomb-origami inspired triboelectric nanogenerator for smart pavement-integrated traffic monitoring. *Nano Res.* **2022**, *15*, 5450–5460.

[27] Zhang, B. B.; Wu, Z. Y.; Lin, Z. M.; Guo, H. Y.; Chun, F.; Yang, W. Q.; Wang, Z. L. All-in-one 3D acceleration sensor based on coded liquid-metal triboelectric nanogenerator for vehicle restraint system. *Mater. Today* **2021**, *43*, 37–44.

[28] Dai, K. R.; Wang, X. F.; Yi, F.; Jiang, C.; Li, R.; You, Z. Triboelectric nanogenerators as self-powered acceleration sensor under high-*g* impact. *Nano Energy* **2018**, *45*, 84–93.

[29] Kim, B.; Song, J. Y.; Kim, D. Y.; Cho, M. W.; Park, J. G.; Choi, D.; Lee, C.; Park, S. M. Environmentally robust triboelectric tire monitoring system for self-powered driving information recognition via hybrid deep learning in time-frequency representation. *Small* **2024**, *20*, 2400484.

[30] Liu, Y. F.; Li, D.; Hou, Y.; Wang, Z. L. Grating-structured freestanding triboelectric nanogenerator for self-powered acceleration sensing in real time. *Adv. Mater. Technol.* **2023**, *8*, 2200746.

[31] Pang, Y. K.; Li, X. H.; Chen, M. X.; Han, C. B.; Zhang, C.; Wang, Z. L. Triboelectric nanogenerators as a self-powered 3D acceleration sensor. *ACS Appl. Mater. Interfaces* **2015**, *7*, 19076–19082.

[32] Le, C. D.; Nguyen, T. H.; Vu, D. L.; Vo, C. P.; Ahn, K. K. A rotational switched-mode water-based triboelectric nanogenerator for mechanical energy harvesting and vehicle monitoring. *Mater. Today Sustain.* **2022**, *19*, 100158.